Organic Electronics 52 (2018) 206–212

Contents lists available at ScienceDirect

Organic Electronics

journal homepage: www.elsevier.com/locate/orgel

Scanning Kelvin Probe Microscopy investigation of the contact resistances and charge mobility in n-type PDIF-CN_2 thin-film transistors

Federico Chianese[a,b,*], Fabio Chiarella[b,a], Mario Barra[b,a], Antonio Carella[c], Antonio Cassinese[a,b]

[a] Physics Department, University of Naples 'Federico II', Piazzale Tecchio, 80, I-80125 Naples, Italy
[b] SPIN-CNR Division of Naples, Piazzale Tecchio, 80, I-80125 Naples, Italy
[c] Chemistry Department, University of Naples 'Federico II', Via Cinthia, I-80125 Naples, Italy

ARTICLE INFO

Keywords:
N-type organic thin-film transistors
Perylene diimides
Scanning Kelvin Probe Microscopy
Contact resistances

ABSTRACT

In this paper, Scanning Kelvin Probe Microscopy (SKPM) was applied in combination with standard current-voltage measurements to assess the contact resistance (R_C) effects and to estimate the contact-free charge carrier mobility in n-type transistors based on evaporated films of PDIF-CN_2. This analysis was carried out in particular as a function of the applied polarization voltages. The separate contributions to the R_C phenomenon coming from the injecting (source) and extracting (drain) electrodes were investigated with the possibility to separately analyze the specific electrical behaviour of these two regions. In agreement with previous results, the experimental data here discussed show that the devices under analysis are not simply injected limited. Voltage drops at both the injecting and extracting contacts must be taken into consideration. However, it is worth to mention that for the bottom-contact devices here investigated, a minimum R_C of 5.5 kΩ cm was found in linear regime. These values are significantly lower (i.e. by a factor 5×) than those previously reported for other perylene dimiide thin-film devices with bottom-contact configuration.

1. Introduction

In the past three decades, scientific attention has been actively focused on the possible technological breakthrough of organic electronics and on the effective application of its paradigms, consisting in the production of flexible, low cost and easy-to-process devices for mass consumer electronics [1]. Rapid advancements prompted the development of a wide number of organic devices such as light-emitting diodes (OLEDs) [2], solar cells [3,4], memories [5], light emitting field-effect transistors (OLETs) [6] and field-effect transistors (OFETs) applied as sensors [7] or for the development of complex circuitry [8].

In the field of OFETs, in particular, remarkable improvements have been achieved in terms of reliability and overall electrical response using innovative compounds which, nowadays, can firmly exceed the performances of amorphous silicon devices. However, within the vast family of newly synthesized organic semiconductors [9], the availability of high performing n-type materials, enabling the development of effective CMOS-like organic circuits for integrated electronic systems, has been an issue for long time [10]. In this context, perylene-3,4,9,10-tetracarboxylic acid diimide derivatives, also known as perylene diimides (PDI's) compounds, have gained great attention in the last years, thanks to their capability to exhibit good n-type charge transport and enhanced stability in ambient conditions, enabled by suitable chemical functionalization [11,12]. Within PDI family, the cyano-functionalized PDIF-CN_2, characterized by the insertions of fluorinated chains ($CH_2C_3F_7$) on the imides' positions, has been used for the fabrication of n-type transistors based on solution-crystallized channels [13], high performing single crystals [14], highly ordered thin films deposited by Organic Molecular Beam deposition (OMBD) [15] and Supersonic Molecular Beam Deposition technique (SuMBD) [16,17]. In the best cases, mobility values largely exceeding 1 $cm^2/V{\cdot}s$ have been extracted from the transfer-curves of these devices. Despite these important advances, severe bottlenecks in the electrical performances and a lack of precise knowledge of the basic principles ruling the charge injection and transport in organic semiconductors are still an open issue [18], especially for thin film transistors (OTFTs). The main drawbacks are to date the strong charge trapping phenomena induced by both chemical defects and structural inhomogeneity [19–21], as well as the presence of intrinsic contact resistances (R_C) at the injecting and extracting electrodes. Because of the contact resistances, a part of the applied voltage between the drain and source (V_{ds}) electrodes is lost across the organic/metal interfaces, downgrading the general performances of the device (in particular in the low V_{ds} region) and hindering considerably their miniaturization capabilities towards the sub-

* Corresponding author. Physics Department, University of Naples 'Federico II', Piazzale Tecchio, 80, I-80125 Naples, Italy.
E-mail address: chianese@fisica.unina.it (F. Chianese).

http://dx.doi.org/10.1016/j.orgel.2017.10.021
Received 1 August 2017; Received in revised form 6 October 2017; Accepted 17 October 2017
Available online 20 October 2017

micrometric scale [22]. The physical reasons behind this phenomenon are mainly relatable to the intrinsic characteristics of the heterojunctions forming between the polycrystalline organic films and the metallic electrodes. Firstly, the energetic mismatch between the Fermi level of the metal electrode (E_F) and the LUMO (HOMO) level of the n-type (p-type) gives rise to the formation of interfacial potential barriers which charge carriers must overcome when injected in or extracted from the device active channel. Moreover, in particular for some specific device configurations, morphological aspects associated to the defective growth of the semiconducting film in the vicinity of the electrodes are able to play a dominant role in the consistent enhancement of R_C values [23].

A powerful approach to characterizing the contact resistance effect in OTFTs is to image the potential distribution along the conducting channel during the device operation by Scanning Kelvin Probe Microscopy (SKPM). By using this technique, indeed, contact resistances are directly measured through the acquisition of the potential difference building up between the tip of an AFM cantilever and the sample. In recent years, SKPM has been widely used in determining surface voltage characteristics and contact effects in pentacene [24], P3HT [25] and TPD:PS [26] organic devices, exploiting the advantage to estimate separately the contributions of source and drain electrodes, in contrast with alternative techniques such as the transmission line method [27] and gated four-probe configuration [28].

In this paper, we present a systematic analysis by means of SKPM of the contact resistance phenomena affecting the response of bottom-contact bottom-gate PDIF-CN_2 OTFTs. The investigation here reported is as a natural follow-up of a previous work by Chiarella et al. [29] on a parent perylene diimide derivative (PDI8-CN_2), where, for thermally evaporated films, R_C values were estimated as a function of the semiconductor layer thickness and in view of the gold electrode functionalization by an aromatic thiol self-assembled monolayer. Similarly to what was found in that previous study, we demonstrate that the R_C values in the n-type OTFTs under consideration are strongly dependent on the applied V_{ds} and weakly dependent on V_{gs}. Scanned probe measurements of the local electrostatic potential allowed us to accurately infer the charge carrier mobility in spite of large potential drops present at the injecting and extracting contacts. Both the contact resistance and the charge mobility were studied as function of temperature as well. Finally, SKPM measurements were used to investigate the peculiar behaviours of charge injection and extraction processes occurring in the electrode/organic regions through the related current-electric field (*I-E*) relations.

2. Materials and methods

A standard bottom-contact bottom-gate architecture has been chosen as test device in this work. PDIF-CN_2 films were deposited on the top of square-shaped (1 cm^2) multi-layered structures consisting of a 500 μm thick highly-doped silicon substrate (n^{++}), acting as distributed gate electrode, 200 nm of thermally grown SiO_2 layer as insulating barrier and photolithographically-processed 170 nm thick interdigitated Au electrodes defining active channels with length $L = 20$ μm and width $W = 11$ mm ($W/L = 550$). The electrode profile is characterized on both sides by a transition region with an initial gradual sloping which is then interrupted abruptly by a down step of about 80 nm (see the lower panel of Fig. 1(c)). Prior the organic film deposition, the dielectric surface was treated with hexamethyldisilazane (HMDS) through an accurate protocol described in detail in Ref. [30]. It is important to stress that HMDS action limits primarily the intrusion of water molecules at the organic/dielectric interface improving consequently the device performances by reducing bias-stress effects both in accumulation and depletion operation modes [21]. Moreover, the SiO_2 surface functionalization by the HMDS self-assembling monolayer enhances the overall morphological quality of the PDIF-CN_2 films [15].

In this work, 25 nm thick PDIF-CN_2 films were grown by Organic Molecular Beam Deposition (OMBD) technique in high vacuum conditions ($P = 10^{-7}$ mbar). The organic powder (Polyera ActivInk N1100) was evaporated by means of a Knudsen cell kept at 220 °C, providing a deposition rate of 0.3 nm/min. The substrate was kept at about 105 °C in order to optimize the film growth mode and guarantee an enhanced electrical response in terms of field-effect mobility [31].

A preliminary electrical characterization of the fabricated PDIF-CN_2 OTFT was performed both in air and in vacuum by using a Janis Probe Station connected to a Keythley 2612A Dual Channel source-meter. In first approximation, it is possible to apply the standard MOSFET theory [32] to model the OTFT response and to extract the field-effect mobility values from the transfer characteristics in linear regime ($|V_{ds}| \ll |V_{gs} - V_{th}|$):

$$\mu_{lin} = \frac{\partial I_{ds}}{\partial V_{gs}} \frac{L}{WC_{ox}} \frac{1}{V_{ds}} \quad (1)$$

and in the saturation regime ($|V_{ds}| \geq |V_{gs} - V_{th}|$):

$$\mu_{sat} = \left(\frac{\partial \sqrt{I_{ds}}}{\partial V_{gs}} \right)^2 \frac{2L}{WC_{ox}} \quad (2)$$

where L and W indicate the channel length and width, respectively, C_{ox} is the oxide capacitance per unit of area, I_{ds} and V_{ds} are the drain-source current and the drain-source applied voltage, respectively. V_{gs} indicates the gate-source voltage while V_{th} is the threshold voltage. It should be pointed out, however, that although the gradual channel approximation can be considered satisfied in our system (i.e. channel length $L = 20$ μm is much larger than oxide thickness $d = 200$ nm), standard MOSFET theory does not take into account the possible trapping effect at the oxide/organic semiconductor interface [33] or the occurrence of non-ohmic processes at the source and drain contacts. For these reasons, careful attention must be paid when interpreting characteristic parameters of OTFTs, such as field-effect mobility [34] or threshold voltage [35], by using eqs. (1) and (2).

In this study, Amplitude Modulation Scanning Kelvin Probe Microscopy (AM-SKPM) measurements were performed by a XE-100 Park atomic force microscope equipped with Cr/Au-coated conducting cantilevers (NSC14 Cr/Au MicroMask$^{(tm)}$). SKPM profiles were acquired in Argon atmosphere, in dual frequency mode (i.e. acquiring simultaneously both the height profile and the potential profile of the OTFT active channel) and biasing the drain and gate electrodes. At the same time, the current was monitored in order to control the device stability. Variable temperature measurements were obtained using a heated scanner in the range 300–380 K. Further details on the acquisition methods and parameters are reported in the Supplementary Material.

3. Results

3.1. Contact resistance evaluation

PDIF-CN_2 OTFTs were firstly tested by standard current–voltage measurements to obtain the output and transfer characteristics. The recorded electrical performances in vacuum were found to be very close to the state-of-the-art results reported for this type of device [11], with maximum mobility values of ~0.5 cm^2/V·s in saturation regime. Similarly to what usually found for most OTFT configurations and even excluding the contact resistance (R_C) effects (see the discussion in the following), mobility in saturation regime is more than doubled in comparison with the highest values ($\mu_{max} \sim 0.2$ cm^2/V·s) extracted in linear regime. On the other hand, the threshold voltages (V_{th}) for these devices are negative and range between −10 and 0 V, being this feature typically ascribed to the large electronic affinity of the Perylene diimide compounds [21].

Representative output curves acquired in vacuum are shown in Fig. 1(a) and (b) where, for V_{ds} approaching to zero, the influence of the

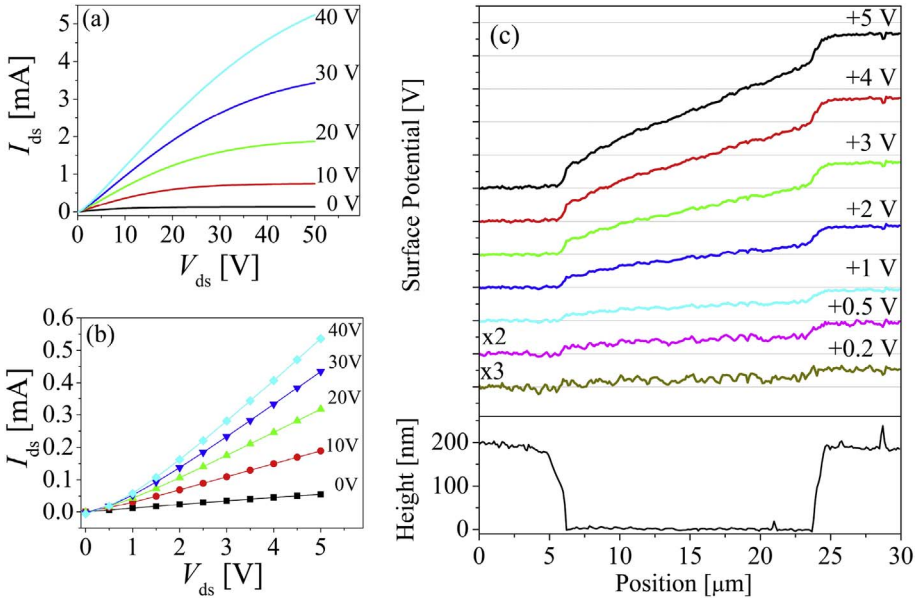

Fig. 1. (a) Typical output curves acquired in vacuum for 0 V < V_{gs} < 40 V. **(b)** Output curves for low drain-source field (0 V < V_{ds} < 5 V). **(c)** Surface potentials for different applied V_{ds} and V_{gs} = 30 V, acquired at room temperature and in Argon saturated atmosphere (upper panel). The correspondent topography of the channel is showed in the lower panel where Source electrode is located on the left and Drain electrode on the right. Surface potential profiles in (c) are shifted (and scaled for V_{ds} = 0.5 and 0.2 V) for clarity. Major ticks spacing along the y-axis in the upper panel is of 1 V.

contact resistance phenomenon gives rise to the generally-observed diode-like (S-shape) behaviour. Here, the channel (I_{ds}) current deviates considerably from the linear trend predicted by the standard MOSFET model, revealing the presence of the parasitic contact effects which tend to hinder the charge injection and/or extraction processes at the PDIF-CN_2/gold interfaces [36]. As a result, the scaling behaviour of the transfer curves is highly dependent on the applied V_{ds} voltages and the effective field-effect mobility (μ_{FET}) in linear regime is strongly decreasing at reducing V_{ds}. In order to quantify the R_C contribution to the overall response of the device and gain eventually insights about the charge transfer mechanisms operating at metal/organic interfaces, surface voltage profiles across the active channel were imaged by means of SKPM during the device operation. Typical potential profiles, acquired at room temperature while keeping the gate bias (V_{gs}) fixed at 30 V and varying the drain-source (V_{ds}) voltage between 0.2 V and 5 V, are reported in Fig. 1(c). For any fixed bias condition, multiple lines were recorded on the same section of the active channel and then averaged in order to minimize the instrumental noise (~20 mV). Nevertheless, it is worth to mention that in AM-SKPM measurements, a systematic underestimation of the measured surface voltage could occur due long-range capacitive coupling of the cantilever [37]. Surface voltage profiles in Fig. 1(c) reveal that the active channel of the investigated OTFT can be electrically described as the series of three different resistive regions. The two voltage drops at the metal/organic interfaces manifest the presence of contact effects, while the central part responds linearly to the externally applied V_{ds} accordingly to the MOSFET model. Moreover, the voltage drops (ΔV_d, ΔV_s) in correspondence of the drain and source electrodes are dependent on the applied V_{ds} and their percentage weight is considerably enhanced (see below) while reducing V_{ds}.

After acquiring the voltage profiles, the contact resistance values at the source (R_s) and drain (R_d) electrodes, expressed in kΩ·cm in order to facilitate the comparison with other data reported in literature, were evaluated by simply dividing the corresponding voltage drops (ΔV_s, ΔV_d) by the width-normalized current density I_{ds}/W. Hence, the overall R_C contribution was achieved through the sum of these terms ($R_C = R_s + R_d$). As shown in Fig. 2(a), the contact resistance values for the devices under investigation were found to display a strongly increasing behaviour when V_{ds} is decreased. In particular, for $V_{ds} \leq 1$ V, the Drain appears to be more affected by the contact resistance phenomenon and R_d is quite larger that R_s. For the set of data reported in Fig. 2(a), for example, at V_{ds} = 0.2 V, R_d is about 34 kΩ cm, while R_s is

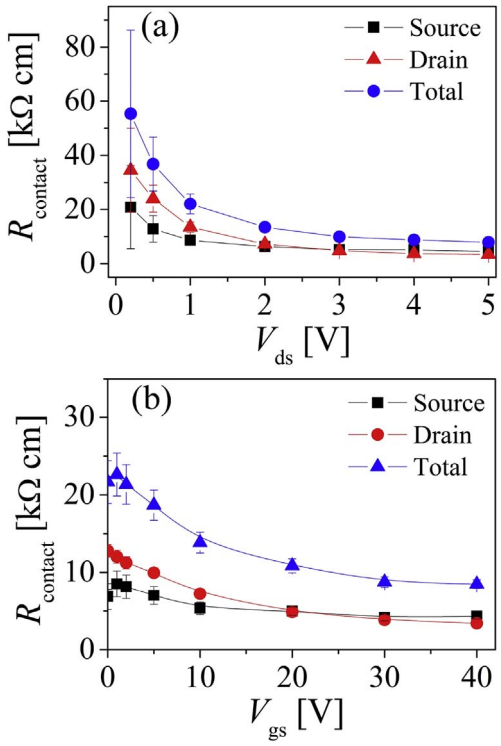

Fig. 2. (a) Behaviour of the contact resistances as function of V_{ds} voltage for a fixed gate-source bias (V_{gs} = 30 V) and **(b)** as function of the gate bias for a fixed drain-source potential (V_{ds} = 5 V).

slightly larger than 20 kΩ cm. Conversely, for V_{ds} values ranging between 3 and 5 V, R_s and R_d exhibit comparable values of few kΩ·cm.

Another general picture about the contact influence on the overall device response is given in the Supplementary Material (see Fig. S1), where the ratio between R_C and the total device resistance (R_{total}, extracted from the output curves) is plotted as function of V_{ds}. Here, for V_{ds} < 2 V, the device is completely contact-limited since the majority of the applied voltage drops across the metal/organic contacts. Beyond the V_{ds} impact, the dependence of the contact resistances on the applied gate voltage (V_{gs}) was also explored, as shown in Fig. 2(b), where R_C values estimated for V_{ds} = 5 V and as a function of V_{gs} are reported. In

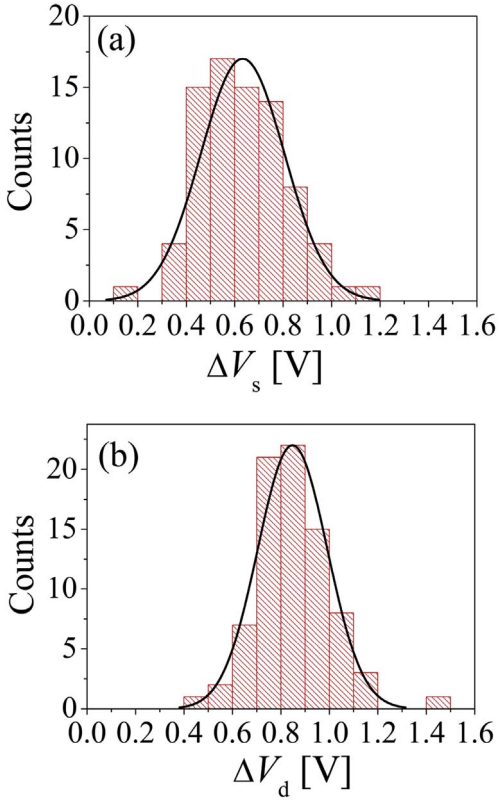

Fig. 3. Statistical distribution of the voltage drops at (**a**) the source and (**b**) drain electrodes for V_{gs} = 30 V and V_{ds} = 5 V.

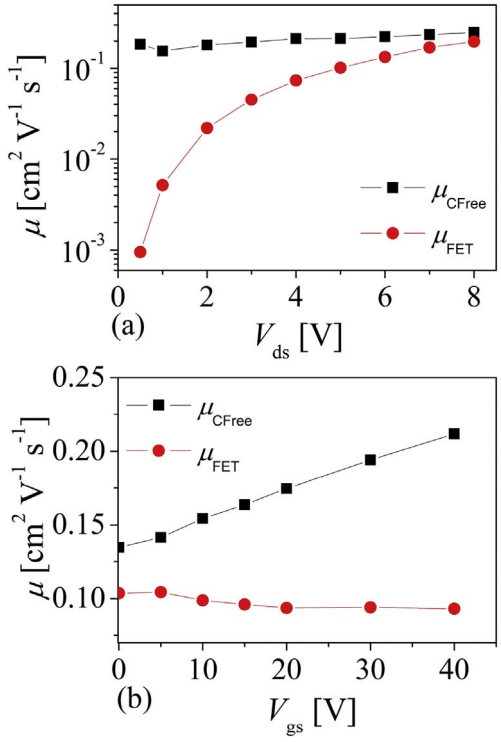

Fig. 4. Comparison between the contact-free mobility (μ_{CFree}) extracted from the SKPM voltage profiles using eq. (3) and the field-effect mobility (μ_{FET}) obtained from linear transfer curves as function of (**a**) V_{ds} for a fixed gate-source bias (V_{gs} = +30 V) and of (**b**) V_{gs} for a fixed drain-source bias (V_{ds} = +5 V).

general, for the investigated devices, a rather weak dependence of R_C on V_{gs} was found, with typical changes by about 40% when V_{gs} goes from 10 to 40 V (namely, this gate voltage range represents the full accumulation region). As a whole, R_C is only slightly modulated by V_{gs} in comparison, in particular, with the theoretical channel resistance behaviour ($R_{ch} \propto 1/(V_{gs}\text{-}V_{th})$).

In order to gain further knowledge about contact phenomena, the local "variability" of the contact resistances was investigated by analyzing various regions of the same device. In this way, we could study the statistical distribution of the voltage drops (ΔV_s, ΔV_d) at the source and drain contacts on a vast area of the OTFT active region. To this aim, ΔV_s and ΔV_d were mapped over *85* different locations of the device, while keeping a fixed polarization (V_{gs} = 30 V and V_{ds} = 5 V) in the linear regime. The observed voltage distributions are shown in Fig. 3(a,b), demonstrating to follow quite well typical Gaussian behaviours. From these data, in particular, the source interface appears to be much more sensitive on the statistical oscillations in comparison with the drain interface. Indeed, while an average voltage drop of 0.6 V and a standard deviation of 0.36 V were observed for the source interface, the same parameters were found to be 0.82 V and 0.20 V, respectively, for the drain electrode [38]. From the statistics on the drain and the source electrodes, assuming the current density to be homogenous along the channel width, an overall average R_C value of 4.9 ± 1.2 k Ω cm is obtained.

3.2. Estimation of the contact-free mobility and temperature effects

The physical identification (see Fig. 1(c)) through the SKPM profiles of the central region of the device channels, where the theoretical linear behaviour is well verified, provides also a direct method to estimate the charge carrier mobility excluding any contact effect. Indeed, by simply extracting from SKPM measurements the voltage value ΔV_{ch} dropping across the central linear zone, the contact-free mobility μ_{CFree} has been calculated as:

$$\mu_{CFree} = \frac{L_{ch} I_{ds}}{W C_{ox}} \times \frac{1}{\Delta V_{ch}(V_{gs} - V_{th})} \quad (3)$$

where L_{ch} indicates the length of the channel central region, W is the overall channel width, I_{ds} is the device current measured during the voltage profile acquisition, C_{ox} the capacitance of the oxide per unit of area and V_{th} is the threshold voltage.

As reported in Fig. 4, μ_{CFree} appears to be basically independent on the drain-source voltage, in contrast with what takes place for the field-effect mobility μ_{FET} obtained from the transfer-curves recorded at various V_{ds}. Indeed, μ_{FET} shows a discrepancy larger than two orders of magnitude for low V_{ds} (Fig. 4(a)) with an exponential decrease towards 10^{-3} cm^2/V·s in correspondence of V_{ds} = 0.2 V.

Using the aforementioned approach (see Fig. 4(b)), it was also found that μ_{CFree} tends to increase linearly with the gate voltage (V_{gs}). Such behaviour is commonly associated to the so-called Multiple Trap and Release transport model, where the predicted V_{gs} dependence of mobility is strictly dictated by the amount of charge induced at the dielectric/organic interface and progressively released from shallow traps at rising V_{gs} [39]. On the other hand, Fig. 4(b) highlights the role of the contact resistances which, counterbalancing the aforementioned growth of the contact-free mobility for high V_{gs}, make the field-effect mobility μ_{FET} apparently decreasing with the gate bias.

In order to complete the characterization of the devices under investigation, the surface potentials were measured as a function of temperature from T = 300 K to T = 350 K. At any temperature, the voltage profiles were acquired by keeping the gate potential fixed (V_{gs} = 30 V) and considering V_{ds} = 0.5 V, 3 V and 5 V. The SKPM profiles achieved in this way are plotted in Fig. S2.

Focusing our attention on the voltage drops at the source and drain electrodes, it appears that they display a mild decaying behaviour at increasing temperature which is more evident for V_{ds} = +5 V and +3 V (Fig. 5(a)). In these cases, going from room temperature to 350 K,

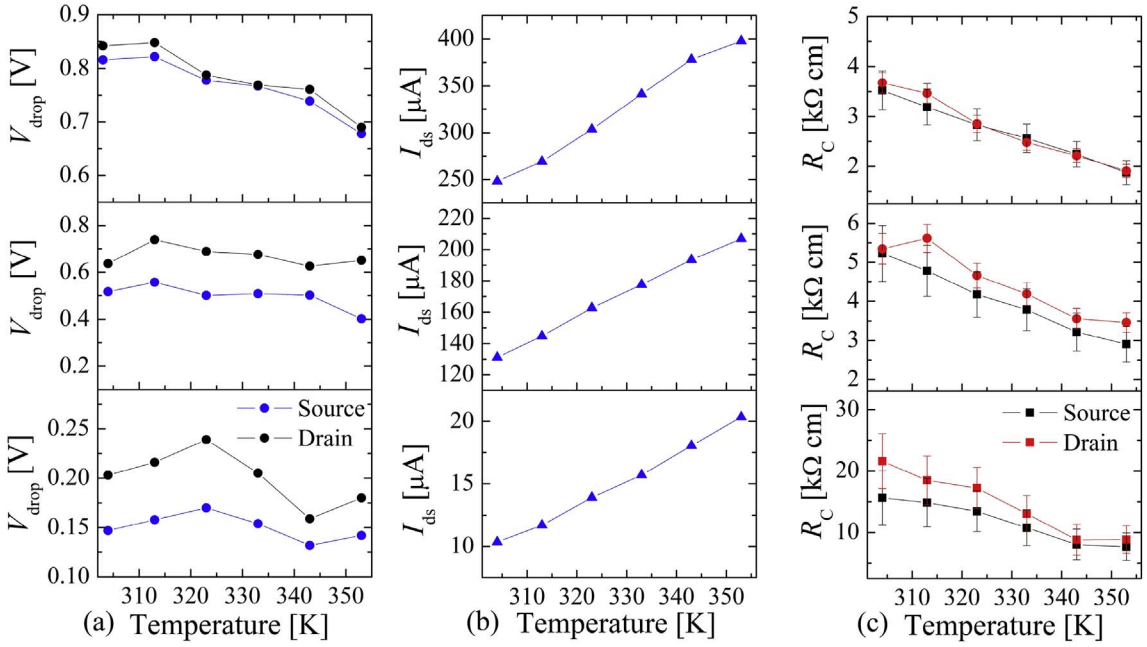

Fig. 5. (a) Voltage drops at the Source and Drain interfaces as function of the temperature. **(b)** Drain-source current and **(c)** contact resistances as function of the temperature and for different bias conditions. For all the images V_{gs} = 30 V while V_{ds} = 0.5 V, 3 V, 5 V starting from the lower panels.

the voltage drops experience a decrement of the order of 18% at both the source and drain interfaces.

On the other hand, the effect of the temperature is much more evident when referring to the charge transport of the device active channel. Indeed, by extracting the contact-free mobility dependence on temperature using this same set of data, we could observe a typical Arrhenius-like behaviour characterized by an activation energy of Δ_E = 107 ± 4 meV. This value was achieved fitting data in Fig. S3 while neglecting the experimental point at 350 K, where thermal instabilities affecting the data reliability were observed in most measurements. It should be outlined that the activation energy here estimated is in good agreement with previously reported data for cyanated perylene diimide compounds [40]. Obviously, this thermal trend is immediately reflected into the I_{ds} currents that undergo to a rapid growth with temperature, at any polarization (Fig. 5(b)). Provided these findings which emphasize the role of the thermally-assisted transport properties of PDIF-CN_2, it is not surprising to observe that the overall trend of contact resistances as function of the temperature is dominated by the I_{ds} current enhancement, giving birth to a general decrement up to 50% for temperatures approaching 350 K (Fig. 5(c)). As a further confirmation of this occurrence, Fig. S3 shows also that the product between R_C and mobility is basically independent on the temperature [41].

4. Discussion

In qualitative terms, the phenomenology of contact resistances here observed for PDIF-CN_2 OTFT seems to agree very well with the results previously reported for PDI8-CN_2 devices having the same configuration [29]. In fact, for both cases, we have found that R_C values are strongly dependent on the polarization conditions and tend to rise consistently when the I_{ds} current flowing through the active channel is reduced (i.e. when V_{ds} and/or V_{gs} are lowered, with the former playing the major role). Consequently, for the devices under consideration, the definition of "contact resistances" is to be meant only as "differential" resistances, implying that the polarization conditions should be defined. It has to be stressed, however, that the contact resistances reported in this work are considerably lowered in comparison with the values observed in Ref. [29]. Indeed, the overall R_C values estimated at very low V_{ds} for PDIF-CN_2 are smaller by more than a factor 2× in comparison with those found for PDI8-CN_2 devices. Even larger improvements (up to a factor 5×) were found at increasing V_{ds}, taking into account that, in this study, R_C at V_{ds} = 5 V was usually comprised between 5 and 10 KΩ cm.

Given these findings, it is evident that, in these systems, there is a relation of inverse proportionality between the estimated R_C and the mobility values. Indeed, while for PDI8-CN_2 OTFT based on evaporated active channels maximum mobility values of 0.1 $cm^2/V{\cdot}s$ are usually found, μ is increased by a factor of 6× when PDIF-CN_2 transistors fabricated with similar processes are considered. In the past, the relation $R_C \propto 1/\mu$ was experimentally observed for several organic transistor configurations and was mainly explained within the theoretical framework of general diffusion-limited thermionic (DLT) phenomena as discussed by Malliaras et al. [42,43]. More recently, this model has been further investigated by Liu et al. [44], to describe the diffusion-limited injection mechanisms occurring for several organic compounds and related device architectures. Within this model, interfacial emission mechanisms are discussed in terms of net interfacial current resulting from the balance between unipolar recombination of charge carriers at the electrode interfaces and thermionic emission of charge in thermal hopping systems, i.e. organic semiconductors, mediated by the presence of a micrometric buffer region in the vicinity of the electrodes where majority carriers are depleted [45]. The resulting behaviour of the overall contact resistances as function of the applied V_{ds} voltage is described by an exponential function of the type:

$$Rc \approx A * \exp(-B\sqrt{V_{DS}}) + R_0 \quad (4)$$

where the fitting parameter A is strictly related to the effective energy barrier at the interfaces ϕ_{eff} following the relation $A \propto (N_0\mu)^{-1}\exp(\varphi_{eff}/kT)$. Here, N_0 indicates the average density of hopping sites in the organic semiconductors. Despite eq. (4) can be satisfactorily applied (not shown here) to shape the experimental R_C data found in this work, the contact resistance phenomenon affecting our devices cannot be explained by simply invoking the DLT model. Indeed, as demonstrated by the analysis of the SKPM profiles, the PDIF-CN_2 devices considered in this work are not just "injection-limited", since the values of R_s and R_d are at least comparable, with the latter becoming even dominant at low V_{ds}. This consideration is further

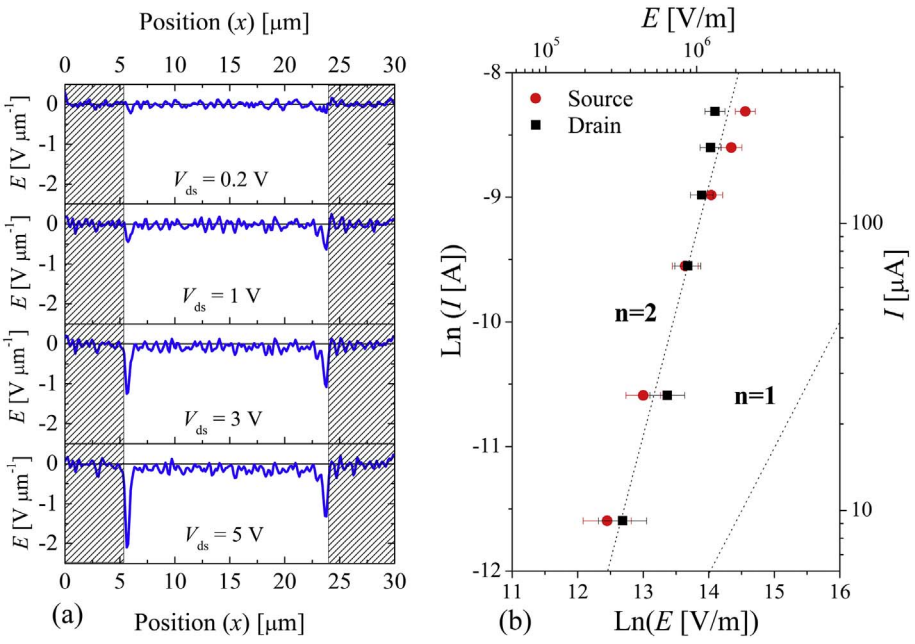

Fig. 6. (a) Calculated electric field profiles over the channel for different V_{ds} (0.2 V < V_{ds} < 5 V). The black patterned edges indicate the source (left) and drain (right) interfaces. The electric field E inside the active channel appears to flicker around average values of E_{avg} = −0.14, −0.07, −0.015, -10^{-4} Vμ^{-1} for V_{ds} = 5, 3, 1, 0.2 V respectively. **(b)** Natural logarithm of the current vs. natural logarithm of the electric field in the access regions close the drain (circles) and source (squares) electrodes. These curves were deduced considering the maximum interfacial electric field values for different V_{ds}. The upper x-axis and the right y-axis indicate the corresponding electric field values expressed in V/m and the drain-source current values expressed in μA, respectively.

supported by the findings of the variable temperature experiments, demonstrating that R_C values follow a thermally activated behaviour with an activation energy being practically the same of the charge carrier mobility and, hence, lower than what predicted by the DLT models as discussed in Ref. [41] and in Ref. [26] where the energetic disorder is also taken into account.

Quite significantly, in fact, in this study we did not observe by AFM (see Fig. S4) remarkable differences (i.e. size and/or shape of the crystalline domains) in the film morphology for distances comparable with those identified in the SKPM profiles (i.e. several hundreds of nanometers).

In order to gain more insights about the physical reasons ruling the observed effects, we analyzed the local correlation between the electric field distribution along the channel in accumulation mode and the related I_{ds} current flowing across the device. The longitudinal electric field (E) across the entire active channel has been calculated by numerical derivation of the acquired surface voltage profiles, i.e. $E = -\partial V/\partial x$ (Fig. 6(a)) where x is the scanning direction along the channel.

In the regions close the electrodes, the electric field appears highly peaked and absolute values as high as 2 V μm^{-1} for E are observed to build up in proximity of the Source contact. Since the electrode/organic interfaces and the central channel are electrically in series and, hence, crossed by the same I_{ds} current, the I-E characteristics related to the source and the drain access regions were obtained (Fig. 6(b)). From the ln-ln plot of these data, we can notice that the currents do not exhibit a linear trend with E, but, rather, their slopes follow closer a quadratic behaviour (n = 2) which is commonly ascribed to Space-Charge-Limited Conduction (SCLC) mechanism [46].

Summarizing, in the OTFT accumulation mode, while the central channel behaves ideally displaying a quite linear dependence between the current and the existing electric field, the access regions near the gold electrodes are characterized by significantly inferior charge transport features. Hence, these two semi-insulating charge-depleted regions, connecting the electrodes and the central conducting channel, exhibit a non-linear electrical response. The presence of SCLC conduction mechanism [46] in the proximity of the source/drain electrodes could be invoked to justify the observed phenomenology. However, alternative explanation cannot be excluded and, in particular, the observed supralinear dependence of the injected and extracted current on the electric field, could be ascribed to the longitudinal electric field dependence of charge carrier mobility in organic semiconductors, as reported by Silveira et al. [47]. Lastly, our experimental data suggest that, if present, the theoretically predicted energy barrier at the injecting electrode (~0.5 eV) seems to have a minor effect respect to the observed injection and extraction mechanisms. Hence, the occurrence of a different energy alignment at the PDIF-CN_2/Gold interface, in which the role of energetic disorder is dominant, should be hypothesized [26,29].

5. Conclusions

In conclusion, in this work, the contact resistance (R_C) effects in PDIF-CN_2-based bottom-contact bottom-gate OTFTs have been evaluated by means of Scanning Kelvin Probe Microscopy (SKPM). In agreement with previous results achieved for a parent perylene diimide compound, the performed experiments reveal that, in these devices, contact resistance (R_C) values decrease when the I_{ds} current flowing across the devices is increased. The effect of the applied V_{ds} voltage is, in particular, quite remarkable. The careful inspection of the surface voltage profiles acquired during the device operation allowed us to evaluate also the charge carrier mobility excluding any contact-related contribution. Interestingly, the contact resistance at the drain electrode was found to dominate for longitudinal electric fields approaching to zero, contradicting the most direct theoretical picture according to which the operation of these devices is purely injection-limited at the source contact. As a general result of this investigation, contact effects appear to be ascribable basically to the electronic properties of the organic film regions (extending for several hundreds of nanometers) in the proximity of the gold electrodes. Apparently, the discussed experimental data cannot be justified only in terms of morphological arguments, being more compatible with a scenario where energetic disorder, space-charge-limited conduction phenomena and the longitudinal electric field dependence of charge carrier mobility could provide the most significant contribution to the R_C phenomenon in the low V_{ds} region.

Notes

The authors declare no competing financial interest.

Acknowledgments

Financial support from INFN-CNR national project (PREMIALE 2012) EOS "Organic Electronics for Innovative research instrumentation" is gratefully acknowledged.

Appendix A. Supplementary data

Supplementary data related to this article can be found at http://dx.doi.org/10.1016/j.orgel.2017.10.021.

References

[1] H. Sirringhaus, 25th anniversary article: organic field-effect transistors: the path beyond amorphous silicon, Adv. Mater. 26 (2014) 1319–1335, http://dx.doi.org/10.1002/adma.201304346.
[2] S. Reineke, F. Lindner, G. Schwartz, N. Seidler, K. Walzer, B. Lüssem, K. Leo, White organic light-emitting diodes with fluorescent tube efficiency, Nature 459 (2009) 234–238, http://dx.doi.org/10.1038/nature08003.
[3] P. Peumans, S. Uchida, S.R. Forrest, Efficient bulk heterojunction photovoltaic cells using small-molecular-weight organic thin films, Nature 425 (2003) 158–162, http://dx.doi.org/10.1038/nature01949.
[4] X. Gu, Y. Zhou, K. Gu, T. Kurosawa, Y. Guo, Y. Li, H. Lin, B.C. Schroeder, H. Yan, F. Molina-Lopez, C.J. Tassone, C. Wang, S.C.B. Mannsfeld, H. Yan, D. Zhao, M.F. Toney, Z. Bao, Roll-to-Roll printed large-area all-polymer solar cells with 5% efficiency based on a low crystallinity conjugated polymer blend, Adv. Energy Mater. 7 (2017) 1–13, http://dx.doi.org/10.1002/aenm.201602742.
[5] T. Sekitani, T. Yokota, U. Zschieschang, H. Klauk, S. Bauer, K. Takeuchi, M. Takamiya, T. Sakurai, T. Someya, Organic nonvolatile memory transistors for flexible sensor arrays, Science 326 (2009) 1516–1519, http://dx.doi.org/10.1126/science.1179963.
[6] S. Toffanin, R. Capelli, W. Koopman, G. Generali, S. Cavallini, A. Stefani, D. Saguatti, G. Ruani, M. Muccini, Organic light-emitting transistors with voltage-tunable lit area and full channel illumination, Laser Photonics Rev. 7 (2013) 1011–1019, http://dx.doi.org/10.1002/lpor.201300066.
[7] O. Knopfmacher, M.L. Hammock, A.L. Appleton, G. Schwartz, J. Mei, T. Lei, J. Pei, Z. Bao, Highly stable organic polymer field-effect transistor sensor for selective detection in the marine environment, Nat. Commun. 5 (2014) 2954, http://dx.doi.org/10.1038/ncomms3954.
[8] V. Subramanian, J.M.J. Fréchet, P.C. Chang, S. Member, D.C. Huang, J.B. Lee, S. Member, S.E. Molesa, S. Member, A.R. Murphy, D.R. Redinger, S. Member, S.K. Volkman, Progress toward development of all-printed RFID tags, Mater. Process. Devices 93 (2005), http://dx.doi.org/10.1109/JPROC.2005.850305.
[9] C. Wang, H. Dong, W. Hu, Y. Liu, D. Zhu, Semiconducting π-Conjugated Systems in Field-Effect Transistors:a material odyssey of organic electronics, Chem. Rev. (2012) 2208, http://dx.doi.org/10.1021/cr100380z.
[10] H. Klauk, U. Zschieschang, J. Pflaum, M. Halik, Ultralow-power organic complementary circuits, Nature 445 (2007) 745–748, http://dx.doi.org/10.1038/nature05533.
[11] B.A. Jones, A. Facchetti, M.R. Wasielewski, T.J. Marks, Tuning orbital energetics in arylene diimide semiconductors. Materials design for ambient stability of n-type charge transport, J. Am. Chem. Soc. 129 (2007) 15259–15278, http://dx.doi.org/10.1021/ja075242e.
[12] R. Centore, L. Ricciotti, A. Carella, A. Roviello, M. Causà, M. Barra, F. Ciccullo, A. Cassinese, Perylene diimides functionalized with N-thiadiazole substituents: synthesis and electronic properties in OFET devices, Org. Electron 13 (2012) 2083–2093, http://dx.doi.org/10.1016/j.orgel.2012.06.002.
[13] J. Soeda, T. Uemura, Y. Mizuno, A. Nakao, Y. Nakazawa, A. Facchetti, J. Takeya, High electron mobility in air for N,N'-1H,1H- perfluorobutyldicyanoperylene carboxydi-imide solution-crystallized thin-film transistors on hydrophobic surfaces, Adv. Mater. 23 (2011) 3681–3685, http://dx.doi.org/10.1002/adma.201101467.
[14] A.S. Molinari, H. Alves, Z. Chen, A. Facchetti, A.F. Morpurgo, High electron mobility in vacuum and ambient for PDIF-CN_2 single-crystal transistors, J. Am. Chem. Soc. 131 (2009) 2462–2463, http://dx.doi.org/10.1021/ja809848y.
[15] F. Chiarella, M. Barra, L. Ricciotti, A. Aloisio, A. Cassinese, Morphology, electrical performance and potentiometry of PDIF-CN_2 thin-film transistors on HMDS-treated and bare silicon dioxide, Electronics 3 (2014) 76–86, http://dx.doi.org/10.3390/electronics3010076.
[16] F. Chiarella, T. Toccoli, M. Barra, L. Aversa, F. Ciccullo, R. Tatti, R. Verucchi, S. Iannotta, A. Cassinese, High mobility n -type organic thin-film transistors deposited at room temperature by supersonic molecular beam deposition, Appl. Phys. Lett. 104 (2014), http://dx.doi.org/10.1063/1.4870991.
[17] F. Chiarella, F. Chianese, M. Barra, L. Parlato, T. Toccoli, A. Cassinese, Spontaneous wetting dynamics in perylene diimide n-type thin films deposited at room temperature by supersonic molecular beam, J. Phys. Chem. C 120 (2016) 26076–26082, http://dx.doi.org/10.1021/acs.jpcc.6b07310.
[18] H. Bässler, A. Köhler, Charge transport in organic semiconductors, Top. Curr. Chem. 312 (2012) 1–65, http://dx.doi.org/10.1007/128_2011_218.
[19] L.M. Smieska, Z. Li, D. Ley, A.B. Braunschweig, J.A. Marohn, Trap-clearing spectroscopy in perylene diimide derivatives, Chem. Mater. 28 (2016) 813–820, http://dx.doi.org/10.1021/acs.chemmater.5b04025.
[20] R.J. Chesterfield, J.C. McKeen, C.R. Newman, C.D. Frisbie, P.C. Ewbank, K.R. Mann, L.L. Miller, Variable temperature film and contact resistance measurements on operating n-channel organic thin film transistors, J. Appl. Phys. 95 (2004) 6396–6405, http://dx.doi.org/10.1063/1.1710729.
[21] F.V. Di Girolamo, F. Ciccullo, M. Barra, A. Carella, A. Cassinese, Investigation on bias stress effects in n-type PDI8-CN 2 thin-film transistors, Org. Electron 13 (2012) 2281–2289, http://dx.doi.org/10.1016/j.orgel.2012.06.044.
[22] A. Hoppe, D. Knipp, B. Gburek, A. Benor, M. Marinkovic, V. Wagner, Scaling limits of organic thin film transistors, Org. Electron 11 (2010) 626–631, http://dx.doi.org/10.1016/j.orgel.2010.01.002.
[23] M. Rapisarda, S. Calvi, A. Valletta, G. Fortunato, L. Mariucci, The role of defective regions near the contacts on the electrical characteristics of bottom-gate bottom-contact organic TFTs, J. Disp. Technol. 12 (2016) 252–257, http://dx.doi.org/10.1109/JDT.2015.2466531.
[24] K.P. Puntambekar, P.V. Pesavento, C.D. Frisbie, Surface potential profiling and contact resistance measurements on operating pentacene thin-film transistors by Kelvin probe force microscopy, Appl. Phys. Lett. 83 (2003) 5539–5541, http://dx.doi.org/10.1063/1.1637443.
[25] L. Bürgi, H. Sirringhaus, R.H. Friend, Noncontact potentiometry of polymer field-effect transistors, Appl. Phys. Lett. 80 (2002) 2913–2915, http://dx.doi.org/10.1063/1.1470702.
[26] T.N. Ng, W.R. Silveira, J.A. Marohn, Dependence of charge injection on temperature, electric field, and energetic disorder in an organic semiconductor, Phys. Rev. Lett. 98 (2007), http://dx.doi.org/10.1103/PhysRevLett.98.066101.
[27] G.K. Reeves, H.B. Harrison, Obtaining the specific contact resistance from transmission line model measurements, IEEE Electron Device Lett. 3 (1982) 111–113, http://dx.doi.org/10.1109/EDL.1982.25502.
[28] P.V. Pesavento, R.J. Chesterfield, C.R. Newman, C.D. Frisble, Gated four-probe measurements on pentacene thin-film transistors: contact resistance as a function of gate voltage and temperature, J. Appl. Phys. 96 (2004) 7312–7324, http://dx.doi.org/10.1063/1.1806533.
[29] F. Chiarella, M. Barra, A. Carella, L. Parlato, E. Sarnelli, A. Cassinese, Contact-resistance effects in PDI8-CN2 n-type thin-film transistors investigated by Kelvin-probe potentiometry, Org. Electron 28 (2016) 299–305, http://dx.doi.org/10.1016/j.orgel.2015.11.009.
[30] M. Barra, D. Viggiano, P. Ambrosino, F. Bloisi, F.V. Di Girolamo, M.V. Soldovieri, M. Taglialatela, A. Cassinese, Addressing the use of PDIF-CN_2 molecules in the development of n-type organic field-effect transistors for biosensing applications, Biochim. Biophys. Acta - Gen. Subj. 1830 (2013) 4365–4373, http://dx.doi.org/10.1016/j.bbagen.2012.11.025.
[31] B.A. Jones, A. Facchetti, M.R. Wasielewski, T.J. Marks, Effects of arylene diimide thin film growth conditions on n-channel OFET performance, Adv. Funct. Mater. 18 (2008) 1329–1339, http://dx.doi.org/10.1002/adfm.200701045.
[32] S. Sze, Semiconductor Devices: Physics and Technology, John Wiley & Sons, 2008.
[33] S.G.J. Mathijssen, M. Kemerink, A. Sharma, M. Cölle, P.A. Bobbert, R.A.J. Janssen, D.M. de Leeuw, Charge Trapping at the Dielectric of Organic Transistors Visualized in Real Time and Space, Adv. Mater. 20 (2008) 975–979, http://dx.doi.org/10.1002/adma.200702688.
[34] E.G. Bittle, J.I. Basham, T.N. Jackson, O.D. Jurchescu, D.J. Gundlach, Mobility overestimation due to gated contacts in organic field-effect transistors, Nat. Commun. 7 (2016) 10908, http://dx.doi.org/10.1038/ncomms10908.
[35] G. Horowitz, R. Hajlaoui, H. Bouchriha, R. Bourguiga, M. Hajlaoui, The concept of "threshold voltage" in organic field-effect transistors, Adv. Mater. 10 (1998) 923–927, http://dx.doi.org/10.1002/(SICI)1521-4095(199808)10:12<923::AID-ADMA923>3.0.CO;2-W.
[36] J.J. Brondijk, F. Torricelli, E.C.P. Smits, P.W.M. Blom, D.M. De Leeuw, Gate-bias assisted charge injection in organic field-effect transistors, Org. Electron. Phys. Mater. Appl. 13 (2012) 1526–1531, http://dx.doi.org/10.1016/j.orgel.2012.04.029.
[37] D.S.H. Charrier, M. Kemerink, B.E. Smalbrugge, T. de Vries, R.A.J. Janssen, Real versus measured surface potentials in scanning Kelvin probe microscopy, ACS Nano 2 (2008) 622–626, http://dx.doi.org/10.1021/nn700190t.
[38] Performing an F-test on the two populations, an F-value of 3.24 ensures with over 99% certainty the actual discrepancy of the two variances.
[39] G. Horowitz, R. Hajlaoui, D. Fichou, A. El Kassmi, Gate voltage dependent mobility of oligothiophene field-effect transistors, J. Appl. Phys. 85 (1999) 3202–3206, http://dx.doi.org/10.1063/1.369661.
[40] M. Barra, F.V. Di Girolamo, F. Chiarella, M. Salluzzo, Z. Chen, A. Facchetti, L. Anderson, A. Cassinese, Transport property and charge trap comparison for N-channel perylene diimide transistors with different air-stability, J. Phys. Chem. C 114 (2010) 20387–20393, http://dx.doi.org/10.1021/jp103555x.
[41] L. Bürgi, T.J. Richards, R.H. Friend, H. Sirringhaus, Close Look at Charge Carrier Injection in Polymer Field-effect Transistors vol. 6129, (2003), pp. 1–10, http://dx.doi.org/10.1063/1.1613369.
[42] J.C. Scott, G.G. Malliaras, Charge injection and recombination at the metal–organic interface, Chem. Phys. Lett. 299 (1999) 115–119, http://dx.doi.org/10.1016/S0009-2614(98)01277-9.
[43] Y. Shen, M.W. Klein, D.B. Jacobs, J. Campbell Scott, G.G. Malliaras, Mobility-dependent Charge Injection into an Organic Semiconductor vol. 86, (2001), http://dx.doi.org/10.1103/PhysRevLett.86.3867.
[44] C. Liu, G. Huseynova, Y. Xu, D.X. Long, W. Park, X. Liu, Universal diffusion-limited injection and the hook effect in organic thin-film transistors, Nat. Publ. Gr (2016) 1–14, http://dx.doi.org/10.1038/srep29811.
[45] D. Khim, K.J. Baeg, M. Caironi, C. Liu, Y. Xu, D.Y. Kim, Y.Y. Noh, Control of ambipolar and unipolar transport in organic transistors by selective inkjet-printed chemical doping for high performance complementary circuits, Adv. Funct. Mater. 24 (2014) 6252–6261, http://dx.doi.org/10.1002/adfm.201400850.
[46] A. Rose, Space-charge-limited currents in solids, Phys. Rev. 97 (1955) 1538–1544, http://dx.doi.org/10.1103/PhysRev.97.1538.
[47] W.R. Silveira, J.A. Marohn, Microscopic view of charge injection in an organic semiconductor, Phys. Rev. Lett. 93 (2004) 2–5, http://dx.doi.org/10.1103/PhysRevLett.93.116104.